

Fast error–controlling MOID computation for confocal elliptic orbits

Roman V. Baluev

Saint Petersburg State University, Faculty of Mathematics and Mechanics, Universitetskij pr. 28, Petrodvorets, Saint Petersburg 198504, Russia

Central Astronomical Observatory at Pulkovo of the Russian Academy of Sciences, Pulkovskoje sh. 65/1, Saint Petersburg 196140, Russia

Denis V. Mikryukov

Saint Petersburg State University, Faculty of Mathematics and Mechanics, Universitetskij pr. 28, Petrodvorets, Saint Petersburg 198504, Russia

arXiv:1811.06373v2 [astro-ph.EP] 29 Dec 2018

Abstract

We present an algorithm to compute the minimum orbital intersection distance (MOID), or global minimum of the distance between the points lying on two Keplerian ellipses. This is achieved by finding all stationary points of the distance function, based on solving an algebraic polynomial equation of 16th degree. The algorithm tracks numerical errors appearing on the way, and treats carefully nearly degenerate cases, including practical cases with almost circular and almost coplanar orbits. Benchmarks confirm its high numeric reliability and accuracy, and that regardless of its error–controlling overheads, this algorithm pretends to be one of the fastest MOID computation methods available to date, so it may be useful in processing large catalogs.

Keywords: close encounters, near-Earth asteroids, NEOs, catalogs, computational methods

1. Introduction

The MOID parameter, or the minimum distance between points on two Keplerian orbits, has an important value in various Solar System studies. It measures the closeness of two trajectories in the \mathbb{R}^3 space, and hence ascertains whether two bodies have a risk to collide. For example, if MOID appeared below the sum of radii of two bodies than such bodies may avoid a collision only if they orbit in a mean-motion resonance, or via a perturbing effect that may increase the MOID to a safe level before the bodies could actually collide. Otherwise, the bodies will necessarily collide in some future.

Therefore, computing the MOID is very old task with an application to Potentially Hazardous Objects (PHOs) and Near-Earth Asteroids (NEAs).

This problem is investigated over decades already, see e.g. (Sitarski, 1968; Dybczyński et al., 1986) and more recent works by Armellin et al. (2010); Hedo et al. (2018).

The MOID is a minimum of some distance or distance-like function $\rho(u, u')$ that depends on two arguments, determining positions on two orbits. The methods of finding the minima of $\rho(u, u')$ can be split in several general categories, depending on the dimensionality of the optimization task to be solved. This depends on how much work is pre-computed analytically.

1. Global optimization in 2D. As an ultimately simple example this includes e.g. the 2D brute-force (exhaustive) search of $\rho(u, u')$ on a 2D grid. Thanks to the existence of rigorous and finite upper limits on the gradient of $\rho(u, u')$, which appears to be a trigonometric polynomial, we can always limit the finite difference

Email address: r.baluev@spbu.ru (Roman V. Baluev)

$\Delta\rho$ by $\Delta u \max |\rho'_u|$ and $\Delta u'$ by $\max |\rho'_{u'}|$. Thanks to such error predictability, algorithms of the 2D class appear the most reliable ones, because we can always determine the MOID, along with the orbital positions u and u' , to any desired accuracy. An advanced method based on the 2D global optimization of ρ , which includes high-order Taylor models and interval arithmetics, was presented by Armellin et al. (2010). Nevertheless, even advanced methods of this type cannot be fast due to the need of considering 2D domains.

2. 1D optimization. Here we eliminate u' from the numeric search by solving it from an analytic equation. The remaining orbital position u is determined by numeric optimization of the 1D function $\tilde{\rho}(u) = \rho(u, u'(u))$. In general, this is faster than 2D minimization, but the derivative of $\tilde{\rho}(u)$ is no longer bounded, because du'/du may turn infinite sometimes. Such cases may appear even for very simple circular orbits. Therefore, in general this method cannot provide a strict mathematical guarantee of the desired numerical accuracy. However, it appears more reliable than the methods of the next class. The SDG method discussed by Hedo et al. (2018) basically belongs to this class.
3. Methods of the 0D class, in which both u and u' are solved for rather than found by numeric optimization. This includes the method by Kholshchevnikov and Vassiliev (1999b) and by Gronchi (2002, 2005), because they do not explicitly deal with any numeric optimization at all. The task is analytically reduced to solving a nonlinear equation with respect to u and then express u' also analytically. Methods of this class are ultimately fast but relatively vulnerable to losing roots due to numerical errors (in nearly degenerate cases). This effect becomes important because the equation for u is quite complicated and subject to round-off errors. Also, this equation often have close (almost multiple) roots that are always difficult for numeric processing.

Here we present an efficient numeric imple-

mentation of the algebraic approach presented by Kholshchevnikov and Vassiliev (1999b), similar to the one presented by Gronchi (2002, 2005). This method belongs to the fast 0D class. It is based on analytic determination of all the critical points of the distance function, $|\mathbf{r} - \mathbf{r}'|^2$, augmented with an algebraic elimination of one of the two positional variables. Mathematically, the problem is reduced to a single polynomial equation of 16th degree with respect to one of the eccentric anomalies.

Recently, Hedo et al. (2018) suggested a method that does not rely on necessary determination of all the stationary points for the distance. It basically splits the problem in two tasks of 1D optimization, so this method belongs to the 1D class. Nevertheless, it proved ~ 20 per cent faster than the 0D Gronchi algorithm, according to the benchmarks. Though the performance differences appeared relatively moderate, there were revealed occurrences when the Gronchi's code suffered from numeric errors, reporting a wrong value for the MOID. Therefore, in this task the numeric reliability of the method is no less important than just the computing speed.

Direct implementation of the methods by Kholshchevnikov and Vassiliev (1999b) and Gronchi (2002) might be vulnerable, because finding roots of a high-degree polynomial might be a numerical challenge sometimes. When dealing with large asteroid catalogs, various almost-degenerate cases appear sometimes, if the equations to be solved contain almost-double or almost-multiple roots. Such roots are difficult to be estimated accurately, because they are sensitive to numeric errors (even if there were no errors in the input orbital elements). Moreover, we have a risk of ambiguity: if the polynomial has two or more very close real roots then numeric errors may result in moving them to the complex plane entirely, so that we may wrongly conclude that there are no such real roots at all. Such effect of lost of real roots may potentially result in overestimating the MOID, i.e. it may appear that we lost exactly the solution corresponding to the global minimum of the distance. This issue can be solved by paying attention not only to the roots formally identified as real, but also to all complex-valued roots that appear suspiciously close to the real axis. To define formally what means 'suspiciously close' we need to estimate

numeric error attached to a given root, not just its formal value.

In other words, our task assigns an increased role to the numeric stability of the computation, because errors are known to dramatically increase when propagating through mathematical degeneracies. This motivated us to pay major attention to error control when implementing the method by Kholshchevnikov and Vassiliev (1999b) in a numerical algorithm.

The structure of the paper is as follows. In Sect. 2, we give some mathematical framework that our algorithm relies upon. Sect. 3 describes the numeric algorithm itself. Sect. 4 contains some guidelines on how to select meaningful error tolerances for our algorithm. Sect. 5 presents its performance tests. In Sect. 6, we describe several auxiliary tools included in our MOID library.

The C++ source code of our MOID library named `DISTLINK` is available for download at <http://sourceforge.net/projects/distlink>.

2. Mathematical setting

Consider two confocal elliptic orbits: \mathcal{E} determined by the five geometric Keplerian elements a, e, i, Ω, ω , and \mathcal{E}' determined analogously by the same variables with a stroke. Our final task is to find the minimum of the distance $|\mathbf{r} - \mathbf{r}'|$ between two points lying on the corresponding orbits, and the orbital positions u, u' where this minimum is attained (here u stands for the eccentric anomaly). According to Kholshchevnikov and Vassiliev (1999b), this problem is reduced to solving for the roots of a trigonometric polynomial $g(u)$ of minimum possible algebraic degree 16 (trigonometric degree 8). It is expressed in the following form:

$$g(u) = K^2(A^2 - C^2)(B^2 - C^2) + 2KC [NA(A^2 - C^2) + MB(B^2 - C^2)] - (A^2 + B^2) [N^2(A^2 - C^2) + M^2(B^2 - C^2)] - 2NMAB, \quad (1)$$

where

$$\begin{aligned} A &= PS' \sin u - SS' \cos u, \\ B &= PP' \sin u - SP' \cos u, \\ C &= e'B - \alpha e \sin u(1 - e \cos u), \\ M &= PP' \cos u + SP' \sin u + \alpha e' - PP'e, \\ N &= PS'e - SS' \sin u - PS' \cos u, \\ K &= \alpha' e'^2, \end{aligned} \quad (2)$$

and $\alpha = a/a'$, $\alpha' = a'/a$. The quantities PP' , PS' , SP' , SS' represent pairwise scalar products of the vectors \mathbf{P} and \mathbf{S} :

$$\begin{aligned} \mathbf{P} &= \{ \cos \omega \cos \Omega - \cos i \sin \omega \sin \Omega, \\ &\quad \cos \omega \sin \Omega + \cos i \sin \omega \cos \Omega, \\ &\quad \sin i \sin \omega \}, \\ \mathbf{S} &= \mathbf{Q} \sqrt{1 - e^2}, \\ \mathbf{Q} &= \{ -\sin \omega \cos \Omega - \cos i \cos \omega \sin \Omega, \\ &\quad -\sin \omega \sin \Omega + \cos i \cos \omega \cos \Omega, \\ &\quad \sin i \cos \omega \}, \end{aligned} \quad (3)$$

with analogous definitions for \mathbf{P}' and \mathbf{S}' .

When all the roots of $g(u)$ are found, for each u we can determine the second position u' from

$$\cos u' = \frac{BC + mA\sqrt{D}}{A^2 + B^2}, \quad \sin u' = \frac{AC - mB\sqrt{D}}{A^2 + B^2}, \quad (4)$$

where

$$D = A^2 + B^2 - C^2, \quad m = \pm 1. \quad (5)$$

The sign of m should be chosen to satisfy

$$M \sin u' + N \cos u' = K \sin u' \cos u', \quad (6)$$

so there is only a single value of u' that corresponds to a particular solution for u .

Finally, after both the orbital positions u and u' were determined, the squared distance between these points is $|\mathbf{r} - \mathbf{r}'|^2 = 2aa'\rho(u, u')$, where

$$\begin{aligned} \rho(u, u') &= \frac{\alpha + \alpha'}{2} + \frac{\alpha e^2 + \alpha' e'^2}{4} - PP'ee' + \\ &\quad + (PP'e' - \alpha e) \cos u + SP'e' \sin u + \\ &\quad + (PP'e - \alpha' e') \cos u' + PS'e \sin u' - \\ &\quad - PP' \cos u \cos u' - PS' \cos u \sin u' - \\ &\quad - SP' \sin u \cos u' - SS' \sin u \sin u' + \\ &\quad + \frac{\alpha e^2}{4} \cos 2u + \frac{\alpha' e'^2}{4} \cos 2u'. \end{aligned} \quad (7)$$

Therefore, our general computation scheme should look as follows: (i) find all real roots of $g(u)$; (ii) for each solution of u determine its corresponding u' ; (iii) for each such pair u, u' compute $\rho(u, u')$; and (iv) among these values of ρ select the minimum one. This will give us the required MOID estimate. As we can see, the most difficult step is finding all real roots of the trigonometric polynomial $g(u)$, while the rest of the work is rather straightforward.

This trigonometric polynomial can be rewritten in one of the two standard forms:

$$g(u) = a_0 + 2 \sum_{k=1}^N (a_k \cos ku + b_k \sin ku) = \sum_{k=-N}^N c_k e^{iku}, \quad (8)$$

where $N = 8$. The coefficients a_k , b_k , and $c_{\pm k} = a_k \mp ib_k$ can be expressed as functions of the quantities PP' , PS' , SP' , SS' , and α , e , e' . Most of such explicit formulae would be too huge and thus impractical, but nonetheless we computed an explicit form for the coefficient c_8 :

$$c_8 = c_{-8}^* = \left(\frac{\alpha e^2}{16} \right)^2 M_1 M_2 M_3 M_4, \\ M_1 = PP' - SS' - ee' - i(SP' + PS'), \\ M_2 = PP' - SS' + ee' - i(SP' + PS'), \\ M_3 = PP' + SS' - ee' - i(SP' - PS'), \\ M_4 = PP' + SS' + ee' - i(SP' - PS'). \quad (9)$$

Here the asterisk means complex conjugation.

The number of real roots of $g(u)$ cannot be smaller than 4 (Kholshchikov and Vassiliev, 1999b). Also, this number is necessarily even, since $g(u)$ is continuous and periodic. But the upper limit on the number of real roots is uncertain. In any case, it cannot exceed 16, the algebraic degree of $g(u)$, but numerical simulations performed by Kholshchikov and Vassiliev (1999b) never revealed more than 12 real roots. Here we reproduce their empirical upper limit: based on a test computation of $\sim 10^8$ orbit pairs from the Main Belt (see Sect. 5), we obtained approximately one 12-root occurrence per $\sim 4 \times 10^6$ orbit pairs¹. No cases with 14 or 16

¹This is actually an upper limit on that rate, because our algorithm may intentionally count some complex roots with small

roots were met.²

Since the number of real roots of $g(u)$ is highly variable and a priori unknown, certain difficulties appear when dealing with $g(u)$ in the real space. In practice $g(u)$ often becomes close to being degenerate, e.g. in the case of almost circular or almost coplanar orbits, which is frequent for asteroids and typical for major planets in the Solar System. In such cases, real roots of $g(u)$ combine in close pairs or even close quadruples. The graph of $g(u)$ passes then close to the abscissa near such roots. This means that numeric computing errors affect such nearly-multiple roots considerably, implying increased uncertainties. Moreover, we might be even uncertain about the very existence of some roots: does the graph of $g(u)$ really intersect the abscissa or it passes slightly away, just nearly touching it? In practice this question may become non-trivial due to numerical errors, that might appear important because $g(u)$ is mathematically complicated. Therefore, treating $g(u)$ only in the real space might result in losing its roots due to numeric errors.

But losing real roots of $g(u)$ would potentially mean to vulnerably overestimate the MOID, because there is a risk that the minimum distance $|r - r'|$ occasionally corresponds to a lost root. Then it might be more safe to overestimate the number of real roots of $g(u)$, i.e. we should also test “almost-real” complex roots that correspond to a near-touching behaviour of $g(u)$, even if it does not apparently intersect the abscissa. This would imply some computational overheads and additional CPU time sacrificed for the algorithmic reliability and numeric stability. Also, this would mean to treat $g(u)$ in the complex plane and find all its complex roots, rather than just the real ones. As such, we need to swap to complex notations.

By making the substitution $z = e^{iu}$ or $w = e^{-iu}$, we can transform $g(u)$ to an algebraic polynomial of

imaginary part as real ones. This estimate is sensitive to the selected floating-point precision and to subtle details that affect overall numeric accuracy of the algorithm. It may even be possible that all these potential 12-root occurrences contain only 10 real roots.

²We had one 14-root occurrence using the standard `DOUBLE` precision, but this case appeared to have only 12 real roots with `LONG DOUBLE` arithmetic.

degree 16:

$$g(u) = \sum_{k=-N}^N c_k z^k = \mathcal{P}(z)w^N = \mathcal{Q}(w)z^N. \quad (10)$$

So, the task of finding roots of $g(u)$ becomes equivalent to solving $\mathcal{P}(z) = 0$ or $\mathcal{Q}(w) = 0$.³ Among all these complex roots we must select those that within numeric errors lie on the unit circle $|z| = |w| = 1$.

Since all a_k and b_k are real, the complex coefficients satisfy the property $c_k = c_{-k}^*$. Hence, roots of $\mathcal{P}(z)$ obey the following rule: if $z = re^{i\varphi}$ is such a root then $1/z^* = r^{-1}e^{i\varphi}$ is also a root of \mathcal{P} . Therefore, the entire set of these roots includes three families: (i) roots on the unit circle $|z| = 1$ that correspond to real u , (ii) roots outside of this circle, $|z| > 1$, and (iii) roots inside the unit circle, $|z| < 1$. The roots with $|z| \neq 1$ are split into pairs of mutually inverse values that have $|z| < 1$ and $|z| > 1$.

3. Numerical algorithm

3.1. Determining the polynomial coefficients and their uncertainty

First of all, we must represent the polynomial $g(u)$ in its canonical form (8). For that, we need to compute the coefficients c_k . The explicit formulae for c_k are too complicated and impractical, except for the case $k = \pm 8$ given in (9). Instead of direct computation of c_k , we determine them by means of the discrete Fourier transform (DFT hereafter):

$$c_k = \frac{1}{2N+1} \sum_{m=0}^{2N} g(u_m) e^{iku_m}, \quad u_m = \frac{2\pi m}{2N+1}. \quad (11)$$

Here, $g(u_m)$ are computed by using the relatively compact formula (1). Regardless of the use of DFT, this approach appears computationally faster than computing all c_k directly. We do not even use FFT algorithms for that, because of too small number of coefficients $N = 8$. For so small N , the FFT technique did not give us any remarkable speed advantage in comparison with the direct application of the DFT (11).

³Since u can take only real values, we always have $z \neq 0$ and $w \neq 0$.

However, the DFT can likely accumulate some rounding errors. The accuracy of so-determined c_k can be roughly estimated by comparing the DFT estimate of $c_{\pm 8}$ with its explicit representation (9), which is still mathematically simple. We may assume that numerical errors inferred by the formula (9) are negligible, and that all the difference between (11) and (9) is solely explained by the DFT errors.

Moreover, we can compute the DFT (11) for any $N > 8$. In such a case, all the coefficients c_k for $|k| > 8$ must turn zero. However, due to numeric errors their DFT estimate may occur non-zero, and in such a case the magnitude of this c_k can be used as a rough error assessment.

Based on this consideration, we adopted the following formulae to estimate the average error in c_k :

$$\varepsilon^2 = \left(|c_8 - c'_8|^2 + \sum_{k=9}^N |c'_k|^2 \right) / (N-7). \quad (12)$$

Here, c_8 is determined from (9), while c'_k are DFT estimations from (11). The formula (12) represents a statistical estimation that treats numerical errors in c_k as random quantities. It is based on the assumption that errors in different c_k are statistically independent (uncorrelated) and have the same variance. In such a case, ε^2 provides an estimate of that variance.

In our algorithm, we set $N = 10$, thus computing the DFT from 21 points u_m . In practical computation we always obtained ε not far from the machine precision, except for rare cases. We additionally notice that the error estimation (12) also includes, to a certain extent at least, the numeric error appeared when computing the values of $g(u_m)$ by formula (1), not just the DFT errors inferred by (11).

3.2. Root-finding in the complex plane

When all c_k are determined, along with their probable numerical error, we can determine all complex roots of $\mathcal{P}(z)$. This is done via Newtonian iterations and obeys the following numeric scheme:

1. Initial approximations for the first 8 roots are selected in a specific optimized manner as detailed below.
2. Initial approximation for each next root z_k is chosen according to the prediction $z_k^{(0)} = 1/z_{k-1}^*$, where z_{k-1} is the final estimation of the

previous root. Thanks to such a choice, the algorithm will always extract a paired complex root $z_k = 1/z_{k-1}^*$ immediately after z_{k-1} . The Newtonian iterations for z_k converge in this case very quickly (in two iterations or so). This does not work, if z_{k-1} belongs to the family $|z| = 1$ (such roots do not combine into inverse pairs), or if z_{k-1} turns out to be that *second* root in the pair. Then such a starting approximation would be equal to either z_{k-1} or z_{k-2} , so the next extracted root z_k will likely appear close to one of these.

3. Each root is refined by Newtonian iterations (i) until some least required relative accuracy δ_{\max} is achieved, and then (ii) until we reach the desired target relative accuracy δ_{\min} or, at least, the maximum possible machine accuracy, if δ_{\min} is unreachable. On the first phase, we iterate until the last Newtonian step $|d_n|$ falls below $\delta_{\max}|z|$. The iterations are restarted from a different starting point, if they are trapped in an infinite loop at this phase (this is the known curse of the Newton method). On the second phase, the stopping criterion relies on the last and pre-last Newtonian steps, $|d_n|$ and $|d_{n-1}|$. The iterations are continued either until $|d_n| < \delta_{\min}|z|$, or until the relative step change, $\gamma_n = (|d_{n-1}|^2 - |d_n|^2)/|d_n|^2$, drops below the machine epsilon ϵ . The latter criterion is motivated as follows. In the middle of iterations, whenever numeric round-off errors are not significant yet, the parameter γ_n should remain large positive, since each $|d_n|$ is much smaller than $|d_{n-1}|$. But in the end either $\gamma_n \rightarrow 0$, if iterations get finally stuck at almost the same numeric value near the root, or γ_n occasionally attains negative values, if the iterations start to randomly jump about the root due to numeric errors. A good practical assumption for the accuracy parameters might be $\delta_{\max} \sim \sqrt{\epsilon}$ and $\delta_{\min} = 0$ or about ϵ .
4. Whenever we have an accurate estimate of a root z_k , this root is eliminated from $\mathcal{P}(z)$ through dividing it by $(z - z_k)$ via the Horner scheme. The remaining polynomial has a reduced degree. For the sake of numerical stability, we either extract the multiplier $(z - z_k)$

from $\mathcal{P}(z)$, if $|z_k| > 1$, or $(w - w_k)$ from $Q(w)$, if $|z_k| < 1$.

5. The roots are extracted in such a way until we receive a quadratic polynomial in $\mathcal{P}(z)$. Its two remaining roots are then obtained analytically.

The order, in which the roots are extracted, is important. If we extract ‘easy’ roots first, we spend little Newtonian iterations with a high-degree \mathcal{P} . Also, such ‘easy’ roots should likely be far from degeneracies and hence be numerically accurate. Therefore, they should not introduce big numeric errors when the Horner scheme is applied. The ‘difficult’ roots that require big number of Newtonian iterations should better be extracted later, when the degree of \mathcal{P} is reduced. If we act in an opposite manner, i.e. extract ‘difficult’ roots first, these difficult roots will inevitably increase numeric errors. After applying the Horner scheme, these increased errors are transferred to the coefficients c_k , reducing the accuracy of all the remaining roots. Also, bad roots always require larger number of Newtonian iterations, which become even more expensive at the beginning, when the degree of \mathcal{P} is still large and its computation is more slow.

After some tests we decided that the best way is to extract in the very beginning extreme complex roots: $|z| \ll 1$ and their inversions $|z| \gg 1$. Such roots are determined quickly and accurately, and the Horner scheme is very stable for them. Since in practical computations we always revealed at least 4 complex roots, we try to extract these four roots in the beginning. The starting approximation for the first root, $z_1^{(0)}$, is always set to zero. This will likely give us the root with smallest $|z_1|$. The next root, z_2 , is started from $z_2^{(0)} = 1/z_1^*$ and will be determined almost immediately. It will be the largest one. Initial approximations for the next two roots, z_3 and z_4 , are set from our usual rule, $z_k^{(0)} = 1/z_{k-1}^*$. Thanks to this, we obtain yet another smallest root as z_3 , and yet another largest root as z_4 .

After these four extreme complex roots are removed from \mathcal{P} , we try to extract the four guaranteed roots that lie on the unit circle. We select their initial approximations to be such that u is located at the orbital nodes or $\pm 90^\circ$ from them. This is motivated by the practical observation that the MOID is usually at-

tained near the orbital nodal line, see Sect. 6. Thanks to such a choice, these four roots are determined in a smaller number of Newtonian iterations.

The ninth root is iterated starting from $z_9^{(0)} = 0$ again, and for the rest of roots we follow the general rule $z_k^{(0)} = 1/z_{k-1}^*$. Thanks to such a choice, the algorithm tries to extract the remaining roots starting far from the unit circle $|z| = 1$, approaching it in the end. Therefore, the most numerically difficult cases, which are usually located at $|z| = 1$, are processed last, when the degree of \mathcal{P} is already reduced in a numerically safe manner.

Using this optimized sequence we managed to reduce the average number of Newtonian iterations from 7–8 per root to 5–6 per root, according to our benchmark test case (Sect. 5). Also, this allowed to further increase the overall numeric accuracy of the roots and numeric stability of the results, because highly accurate roots are extracted first and roots with poor accuracy did not affect them.

3.3. Estimating roots uncertainty and roots selection

When all complex roots of $\mathcal{P}(z)$ are obtained, we need to select those roots that satisfy $|z| = 1$ and thus correspond to real values of u . However, in practice the equation $|z| = 1$ will never be satisfied exactly, due to numerical errors. We need to apply some criterion to decide whether a particular $|z_k|$ is close to unit, within some admissible numeric errors, or not.

We approximate the relative error of the root z_k by the following formula:

$$\varepsilon_z^2 = \frac{1}{|z_k|^2} \left(|d|^2 + \frac{\varepsilon_{\mathcal{P}}^2}{|\mathcal{D}|^2} \right). \quad (13)$$

Its explanation is as follows.

Firstly, d is the smaller (in absolute value) of the roots of a quadratic polynomial that approximates $\mathcal{P}(z)$ near z_k :

$$\begin{aligned} \frac{\mathcal{P}''(z_k)}{2}d^2 + \mathcal{P}'(z_k)d + \mathcal{P}(z_k) &= 0, \\ d = \frac{-\mathcal{P}' + \mathcal{D}}{\mathcal{P}''}, \quad \mathcal{D} &= \pm \sqrt{\mathcal{P}'^2 - 2\mathcal{P}\mathcal{P}''}. \end{aligned} \quad (14)$$

Thus, the first term in (13), or $|d|$, approximates the residual error of z_k still remained after Newtonian iterations. It is zero if $\mathcal{P}(z_k) = 0$ precisely. Here we

use the initial polynomial \mathcal{P} of 16th degree, not the one obtained after dividing it by any of $z - z_k$. For practical purposes, d should be calculated using a numerically stabilized formula that avoids subtraction of close numbers whenever $\mathcal{P} \approx 0$. For example, we can use

$$d = \frac{-2\mathcal{P}}{\mathcal{P}' + \mathcal{D}}, \quad (15)$$

selecting such sign of \mathcal{D} that maximizes the denominator $|\mathcal{P}' + \mathcal{D}|$.

But just $|d|$ is not enough to characterize the uncertainty of z_k in full. In fact, most of this uncertainty comes from the numerical errors appearing in $\mathcal{P}(z)$ through c_k . Inaccurate computation of $\mathcal{P}(z)$ leads to errors in the estimated root z_k . Using the quadratic approximation (14), the sensitivity of z_k with respect to varying \mathcal{P} is expressed by the derivative $\partial d / \partial \mathcal{P} = -1/\mathcal{D}$. Hence, the second error term in (13) appears, $\varepsilon_{\mathcal{P}}/|\mathcal{D}|$, where $\varepsilon_{\mathcal{P}}$ represents the error estimate of $\mathcal{P}(z)$:

$$\varepsilon_{\mathcal{P}}^2 = \varepsilon^2 \sum_{n=0}^{16} |z_k|^{2n}, \quad (16)$$

where ε given in (12).

The quadratic approximation (14) is related to the iterative Muller method that takes into account the second derivative of \mathcal{P} . We needed to take into account \mathcal{P}'' because in practice the real roots of $g(u)$ are often combined into close pairs, triggering a close-to-degenerate behaviour with small $|\mathcal{P}'(z)|$. In such a case the linear (Newtonian) approximation of $\mathcal{P}(z)$ yields too pessimistic error estimate for z_k . The use of the quadratic approximation (14) instead allows us to adequately treat such cases with nearly double roots.

However, even with (14) it is still difficult to treat the cases in which the roots combine in close quadruples. Then $\mathcal{P}''(z_k)$ becomes small too, along with $\mathcal{P}'(z_k)$ and $\mathcal{P}(z_k)$. The error estimate (13) becomes too pessimistic again. Such cases are very rare, but still exist. They may need to be processed with an alternative computation method (see Sect. 6).

In the error estimate (13), we neglect numerical errors of $\mathcal{P}'(z_k)$ and of $\mathcal{P}''(z_k)$, assuming that these quantities do not vanish in general and thus always keep a satisfactory relative accuracy (this is typically true even for almost double paired roots).

We use the following numeric criterion to identify roots lying on the unit circle:

$$\Delta_z = \frac{|\log |z||}{\nu \varepsilon_z} \leq 3. \quad (17)$$

Here, ν is an auxiliary scaling parameter controlling the tolerance of the threshold. Normally, it should be set to unit and its meaning is to heuristically correct the estimated ε_z in case if there are hints that this error estimation is systematically wrong. The threshold 3 is supposed to mean the so-called three-sigma rule. It was selected well above the unit in order to increase the safety of roots selection and hence the reliability of the entire algorithm.

After selecting all the roots z_k that lie close enough to the unit circle, we may determine the corresponding eccentric anomaly $u_k = \arg z_k$, then its corresponding u'_k from (4) and $\rho_k = \rho(u_k, u'_k)$ from (7). The minimum among all computed ρ_k yields us the required MOID estimate.

In general, the discriminant D in (4) is non-negative if u is a root of $g(u)$, but this can be violated in some special degenerate cases (Baluyev and Kholshchevnikov, 2005). Formally, negative D means that MOID cannot be attained at the given orbital position u , even if $g(u) = 0$. This is quite legal, meaning that some roots of $g(u)$ may be parasitic, i.e. corresponding to a critical point of $\rho(u, u')$ for some complex u' (even if u is real). However, D may also turn negative due to numeric errors perturbing almost-zero $D > 0$. We could distinguish such cases based on some uncertainty estimate of D , but in practice it appears easier to process all them just forcing $D = 0$. In the first case (if D is negative indeed), this would imply just a negligible computation overhead because of unnecessary testing of an additional ρ_k that cannot be a MOID. But in the second case (if D appeared negative due to numeric errors) we avoid losing a potential MOID candidate ρ_k .

3.4. Refining the MOID by 2D iterations

Now we have quite a good approximation for the MOID and for the corresponding positions in u and u' . However, their accuracy is typically 1-2 significant digits worse than the machine precision (even

if we iterated the roots z_k to the machine precision). The loss of numeric precision appears in multiple places: in rather complicated formulae like (1), in (4) if D appeared small, in the DFT computation (11), and so on. As a result, whenever working in the standard DOUBLE precision, we may receive average numeric errors of $\sim 10^{-14}$ instead of the relevant machine epsilon $\sim 10^{-16}$. Although this average accuracy is pretty good for the most practical needs, in poorly-conditioned cases the errors may increase further. But fortunately, the results can be easily refined to the machine precision $\sim 10^{-16}$ at the cost of negligible overheads.

This can be achieved by applying the 2D Newton iteration scheme to the function $\rho(u, u')$. Let us decompose it into the Taylor series:

$$\rho(u, u') = \rho_0 + \mathbf{g} \cdot \mathbf{d} + \frac{1}{2} \mathbf{d}^T \mathbf{H} \mathbf{d} + \dots \quad (18)$$

Here, \mathbf{g} is the gradient and \mathbf{H} is the Hessian matrix of ρ , considered at the current point (u, u') , while \mathbf{d} is the 2D step in the plane (u, u') . We need to find such \mathbf{d} where the gradient of (18) vanishes:

$$\nabla \rho = \mathbf{g} + \mathbf{H} \mathbf{d} + \dots = 0, \quad (19)$$

therefore the necessary 2D step is

$$\mathbf{d} = -\mathbf{H}^{-1} \mathbf{g}. \quad (20)$$

To compute ρ , \mathbf{g} , and \mathbf{H} , we do not rely on the formula (7), because it is poorly suited for practical numeric computations. It may generate a precision loss due to the subtraction of large numbers. Such a precision loss appears when MOID is small compared to a and a' .

The derivatives of ρ can be computed using the following formulae, obtained by direct differentiation:

$$\begin{aligned} \rho &= \frac{(\mathbf{r} - \mathbf{r}')^2}{2aa'}, \quad g_u = \frac{(\mathbf{r} - \mathbf{r}') \mathbf{r}_u}{2aa'}, \quad g_{u'} = -\frac{(\mathbf{r} - \mathbf{r}') \mathbf{r}'_{u'}}{2aa'}, \\ H_{uu} &= \frac{(\mathbf{r} - \mathbf{r}') \mathbf{r}_{uu} + \mathbf{r}_u^2}{2aa'}, \quad H_{u'u'} = \frac{(\mathbf{r} - \mathbf{r}') \mathbf{r}'_{u'u'} + \mathbf{r}'_{u'}^2}{2aa'}, \\ H_{uu'} &= -\frac{\mathbf{r}_u \mathbf{r}'_{u'}}{2aa'}, \quad \mathbf{r}_u = \frac{d\mathbf{r}}{du}, \quad \mathbf{r}'_{u'} = \frac{d\mathbf{r}'}{du'}. \end{aligned} \quad (21)$$

In fact, the effect of the precision loss is present in (21) too, due to the difference $\mathbf{r}-\mathbf{r}'$, but formula (7) would exacerbate it further, because it hiddenly involves subtraction of *squares* of the quantities.

Now, according to Baluyev and Kholshchevnikov (2005), the radius-vector \mathbf{r} on a Keplerian elliptic orbit is

$$\frac{\mathbf{r}}{a} = \mathbf{P}(\cos u - e) + \mathbf{S} \sin u, \quad (22)$$

with a similar expression for \mathbf{r}' . The corresponding derivatives with respect to u and u' are obvious.

The stopping criterion for the 2D iterations (20) is similar to the one used in the Newton-Raphson scheme for the roots z_k . It applies the tolerance parameter δ_{\min} to $|\mathbf{d}|$. The iterations are therefore continued either until this accuracy δ_{\min} is reached by the angular variables u and u' , or until we reach the maximum possible numeric precision, so that further iterations unable to increase it. The other control parameter δ_{\max} is not used here.

In practice it appears enough to make just one or two refining iterations (20) to reach almost the machine accuracy in ρ . In rare almost-degenerate cases we may need $n = 3$ iterations or more, but the fraction of such occurrences is small and quickly decreases for larger n .

3.5. Estimating uncertainties of the MOID and of its orbital positions

The numeric errors in u and u' come from three sources: the floating-point ‘storage’ errors, the residual errors appearing due to inaccurate fit of the condition $\nabla\rho = 0$, and the numeric errors appearing when computing \mathbf{g} . Each of these error components transfers to ρ .

The first error part in u, u' can be roughly approximated as

$$\sigma_{u,u'}^{(1)} = \pi\nu\epsilon, \quad (23)$$

assuming that ν is our universal error scaling factor. Since the gradient \mathbf{g} is negligible near the MOID, the Taylor decomposition (18) implies the following error in ρ :

$$\Delta\rho \simeq \frac{1}{2}\mathbf{d}^T\mathbf{H}\mathbf{d}, \quad (24)$$

where \mathbf{d} has the meaning of the 2D numeric error in u, u' . From (23), we know only the typical length of

\mathbf{d} , but the direction of this vector can be arbitrary. Then we can use the Rayleigh inequality

$$|\mathbf{d}^T\mathbf{H}\mathbf{d}| \leq |\lambda_{\max}|\mathbf{d}^2, \quad (25)$$

where λ_{\max} is the maximum (in absolute value) eigenvalue of \mathbf{H} . Since the size of \mathbf{H} is only 2×2 , it can be computed directly:

$$|\lambda_{\max}| = \left| \frac{H_{uu} + H_{u'u'}}{2} \right| + \sqrt{\left(\frac{H_{uu} - H_{u'u'}}{2} \right)^2 + H_{uu'}^2}. \quad (26)$$

So, the indicative uncertainty in ρ coming from this error source is

$$\sigma_{\rho}^{(1)} \simeq \frac{|\lambda_{\max}|}{2} (\sigma_u^{(1)})^2. \quad (27)$$

The second error part in u, u' can be derived from (20), substituting the residual gradient \mathbf{g} that appears after the last refining iteration:

$$\begin{pmatrix} \sigma_u^{(2)} \\ \sigma_{u'}^{(2)} \end{pmatrix} = -\mathbf{H}_{\text{rsd}}^{-1}\mathbf{g}_{\text{rsd}}. \quad (28)$$

From (18), this will imply the following error in ρ :

$$\sigma_{\rho}^{(2)} \simeq \frac{1}{2}\mathbf{g}_{\text{rsd}}^T\mathbf{H}_{\text{rsd}}^{-1}\mathbf{g}_{\text{rsd}}. \quad (29)$$

The third error source comes from possible round-off errors in \mathbf{g} , which may perturbate the computed position of the local minimum of ρ via (20). Let us assume that the numeric uncertainty of \mathbf{g} is σ_g , which has the meaning of a typical length of the computed vector \mathbf{g} at the strict (algebraic) stationary point of ρ , where \mathbf{g} must vanish. Then from (20) one may derive that

$$|\mathbf{d}| \leq \frac{|\mathbf{g}|}{|\lambda_{\min}|}, \quad (30)$$

where the λ_{\min} is the minimum eigenvalue of \mathbf{H} :

$$\frac{1}{|\lambda_{\min}|} = \frac{|\lambda_{\max}|}{|\det\mathbf{H}|}. \quad (31)$$

Hence, the corresponding uncertainty in u, u' is estimated by

$$\sigma_{u,u'}^{(3)} \simeq \frac{|\lambda_{\max}|}{|\det\mathbf{H}|}\sigma_g, \quad (32)$$

The corresponding uncertainty for ρ can be expressed using (29), but now \mathbf{g} is basically an unknown random vector of average length $\sim \sigma_g$. We can again apply the Rayleigh inequality to obtain

$$\sigma_\rho^{(3)} \simeq \frac{|\lambda_{\max}|}{2} \frac{\sigma_g^2}{|\det \mathbf{H}|}. \quad (33)$$

The quantity σ_g appears more complicated and is derived below.

The fourth error source in ρ appears when applying the first formula of (21). If MOID is small then the relative error in ρ increases due to the precision loss, appearing because of the subtraction of close vectors \mathbf{r} and \mathbf{r}' . If these vectors have relative ‘storage’ errors about $\nu\epsilon$ then their absolute numeric errors are $\sigma_r \sim \nu\epsilon r$ and $\sigma_{r'} \sim \nu\epsilon r'$. Hence, the inferred cumulative uncertainty of the difference is about their quadrature sum:

$$\sigma_{r-r'} \simeq \nu\epsilon \sqrt{r^2 + r'^2}. \quad (34)$$

Let us compute the inferred uncertainty in ρ using the so-called delta method. Since $2aa'\rho = (\mathbf{r} - \mathbf{r}')^2$ then the error $\Delta\rho$ appearing due to a small perturbation $\Delta_{r-r'}$ is

$$2aa'\Delta\rho = 2(\mathbf{r} - \mathbf{r}')\Delta_{r-r'} + \Delta_{r-r'}^2. \quad (35)$$

By replacing the terms above with their uncertainties or with absolute values of vectors, and assuming that different terms are always added in the worst-case fashion, the final error component in ρ may be estimated as follows:

$$\sigma_\rho^{(4)} \simeq 2\rho \frac{\sigma_{r-r'}}{\sqrt{2aa'}} + \frac{\sigma_{r-r'}^2}{2aa'}. \quad (36)$$

Notice that we cannot in general neglect the last term in (36), because it may appear significant if ρ is small.

Now we can also estimate the numeric uncertainty of \mathbf{g} by computing its finite difference from (21), analogously to $\Delta\rho$:

$$2aa'\Delta\mathbf{g} \simeq \begin{pmatrix} \Delta_{r-r'}\mathbf{r}_u + (\mathbf{r} - \mathbf{r}')\Delta\mathbf{r}_u \\ \Delta_{r-r'}\mathbf{r}'_u + (\mathbf{r} - \mathbf{r}')\Delta\mathbf{r}'_u \end{pmatrix}. \quad (37)$$

By applying the same approach as for $\Delta\rho$, we may obtain the following for the uncertainties in \mathbf{g} :

$$2aa' \begin{pmatrix} \sigma_{g_u} \\ \sigma_{g'_u} \end{pmatrix} \simeq \begin{pmatrix} \sigma_{r-r'}r_u + \rho \sqrt{2aa'}\sigma_{r_u} \\ \sigma_{r-r'}r'_u + \rho \sqrt{2aa'}\sigma_{r'_u} \end{pmatrix}. \quad (38)$$

Since $\sigma_g^2 = \sigma_{g_u}^2 + \sigma_{g'_u}^2$, and $\sigma_{r_u} \sim \nu\epsilon r_u$, and using (34), one can obtain

$$\sigma_g \simeq \frac{\nu\epsilon}{2aa'} \left(|\mathbf{r} - \mathbf{r}'| + \sqrt{r^2 + r'^2} \right) \sqrt{r_u^2 + r'_u{}^2}. \quad (39)$$

But now we can clearly see that the term $|\mathbf{r} - \mathbf{r}'|$ is either small or of the same order as $\sqrt{r^2 + r'^2}$, so to simplify the formula we can simply neglect it and leave only the latter term. We therefore put:

$$\sigma_g \simeq \frac{\nu\epsilon}{2aa'} \sqrt{r^2 + r'^2} \sqrt{r_u^2 + r'_u{}^2}. \quad (40)$$

This should be substituted to the formula (33) above.

Finally, summing up all four error components in ρ yields the cumulative uncertainty

$$\sigma_\rho \sim \sigma_\rho^{(1)} + \sigma_\rho^{(2)} + \sigma_\rho^{(3)} + \sigma_\rho^{(4)}. \quad (41)$$

Of course, some of these error terms may often become negligible, but it is difficult to predict in advance which terms would dominate in this sum. Since either term may appear large in certain conditions, we need to preserve all of them for the sake of reliability.

After that, an indicative uncertainty for the MOID = $\sqrt{2aa'\rho}$ is approximated by using the delta method as

$$\sigma_{\text{MOID}} \sim \frac{aa'\sigma_\rho}{\text{MOID}}. \quad (42)$$

This formula is valid only if ρ is not close to zero (compared to σ_ρ). Otherwise, the MOID uncertainty is

$$\sigma_{\text{MOID}} \sim \sqrt{2aa'\sigma_\rho}. \quad (43)$$

The two latter formulae can be combined into a single approximate one:

$$\sigma_{\text{MOID}} \sim \frac{aa'\sigma_\rho}{\sqrt{\text{MOID}^2 + aa'\sigma_\rho/2}}. \quad (44)$$

3.6. Self-testing numerical reliability

Finally, our algorithm includes a self-diagnostic test that verifies the following post-conditions:

1. All roots that passed (17) must comply with the requested least accuracy: $\nu\epsilon_z < \delta_{\max}$.

2. The minimum of Δ_z among all the roots that failed (17) must exceed 10, meaning that there is no other suspicious root candidates. That is, the families $|z| = 1$ and $|z| \neq 1$ must be separated by a clear gap.
3. The number of roots that passed (17) must be even and greater than four (necessary algebraic conditions following from the theory).
4. After the 2D refining, the Hessian \mathbf{H}_{rsd} is strictly positive-definite, so we indeed are at a local minimum (rather than maximum or saddle point).
5. On the 2D refining stage, the total cumulative change in u satisfies the condition $|\Delta u| < \delta_{\text{max}}$. In some part this condition duplicates (i), ensuring the initial approximation of the corresponding root did not appear to have unacceptable accuracy. But it also ensures that the 2D refining did not switch us to a completely different root of $g(u)$ (another stationary point of ρ). We pay no attention to u' here, because it is always derived from u using (4), so its numeric error, even if large, is not indicative regarding the selection of a correct root of $g(u)$.

If some of these conditions are broken, the algorithm sets a warning flag. Receiving such a signal, the results should be considered unreliable. In practice this is a very seldom case (see next section), but still possible. Then the following sequence can be done to verify the results: (i) run the same algorithm on the same orbits \mathcal{E} and \mathcal{E}' , but swap them with each other; (ii) if failed again, run the same algorithm using the LONG DOUBLE precision instead of DOUBLE; (iii) run the LONG DOUBLE computation on swapped orbits; (iv) if everything failed, invoke an alternative MOID algorithm, e.g. the one from Sect. 6.

We notice that since the task is solved asymmetrically, the algorithm may yield slightly different results when computing $\text{MOID}(\mathcal{E}, \mathcal{E}')$ and $\text{MOID}(\mathcal{E}', \mathcal{E})$. If the orbital configuration does not imply degeneracies, both computations should offer the same MOID value, within the reported uncertainties. If they differ unacceptably, this can serve as an additional indicator that something went wrong.

However, this notice does not apply to the estimated MOID uncertainty. This uncertainty can

appear different when computing $\text{MOID}(\mathcal{E}, \mathcal{E}')$ and $\text{MOID}(\mathcal{E}', \mathcal{E})$, because the polynomials $g(u)$ and $g(u')$ may have (and usually do have) different algebraic properties. In fact, if the goal is accuracy rather than speed, one may always compute the MOID in the both directions, $\mathcal{E} \rightarrow \mathcal{E}'$ and $\mathcal{E}' \rightarrow \mathcal{E}$, selecting the value offering better accuracy.

4. On the choice of error tolerances

The algorithm involves three main parameters related to the error control: δ_{min} , δ_{max} , and ν .

The primary error tolerance is δ_{min} . It controls the resulting accuracy of the roots z_k , and of the eccentric anomalies u, u' , but not of the MOID itself and not even of the adimensional function ρ . By setting δ_{min} to a larger or smaller value we may obtain less or more accurate result (in terms of u, u'). We can set $\delta_{\text{min}} = 0$, meaning to seek maximum precision possible with the hardware (though this probably requires to use the LONG DOUBLE arithmetic, see below).

The auxiliary error tolerance δ_{max} does not actually control the accuracy of the results. Setting a smaller δ_{max} won't result in a more numerically accurate MOID estimate. This parameter has two aspects: (i) it is used in the root-finding part to control the initial 'burn-in' stage of the Newton scheme and (ii) it is used as an indicative threshold to separate numerically 'reliable' cases from 'unreliable' ones.

Therefore, the common sense requires that δ_{max} must be greater (preferably, significantly greater) than δ_{min} . Forcing δ_{max} too small may result in the following undesired effects. First, the Newton root-finding scheme may drastically slow down, because its 'burn-in' stage does not expect that it may reach the machine precision and may otherwise iterate the roots until the internal iteration limit. The output precision would then be worse than δ_{max} anyway. Secondly, too small δ_{max} may trigger an unnecessary increase of the number of the unreliability warnings.

Concerning the unreliability warnings, the practical value of δ_{max} can be selected based on the observational uncertainty of orbital elements (relative uncertainty in terms of a, a' or absolute one in terms of the angular elements). This input uncertainty is typically considerably larger than the machine precision. With so-selected δ_{max} , the warning flag would indi-

cate that the numeric accuracy of z_k might be worse than the errors inferred by input observational uncertainties. Then the intermediate (inferred by z_k) numeric uncertainty of u and u' may appear larger than what we can trigger by varying the orbital elements within their error boxes. In this case the warning is physically reasonable. But if the numeric uncertainty always remains below the observational one then signaling any warning does not make sense.

In any case, it does not make sense to set δ_{\max} too much below the physical sizes of the objects (relative to $\sim \max(a, a')$). For the Main Belt, this is $\sim 10^{-11}$ AU corresponding to the smallest known asteroids of ~ 1 m in size.

If the uncertainty of orbital elements is unknown or irrelevant than the good choice of δ_{\max} is $\sqrt{\delta_{\min}}$, which follows from the properties of the Newton-Raphson method. In such a case, for each root z_k we need to make just one or two iterations after the ‘burn-in’ part of the Newton scheme. This is because the number of accurate digits is roughly doubled after each Newtonian iteration. For example, if the accuracy of $\sqrt{\epsilon}$ has been reached, on the next iteration we will likely have ϵ .

As to the last control parameter, ν , it may be used to manually scale up all the error assessments. So far in our tests we did not find practical reasons to set it to something different from $\nu = 1$. But whenever necessary, it can be used to disentangle the value δ_{\max} used by the Newtonian root-finding scheme from the threshold used in the error control part. Since ν scales all the error estimates up, its effect is equivalent to reducing the error threshold from δ_{\max} to δ_{\max}/ν , but the Newton scheme is always using δ_{\max} and ignores the scale factor ν .

Summarizing, it appears that in the general case it is reasonable to set δ_{\min} about the machine epsilon, $\delta_{\max} \sim \sqrt{\delta_{\min}}$, and to select such ν that δ_{\max}/ν is about the physically justified MOID uncertainty (relative to $\sim \max(a, a')$).

5. Practical validation and performance benchmarks

We tested our algorithm on the first 10000 numbered asteroids from the Main Belt, implying $\sim 10^8$

orbit pairs. The orbital elements were taken from the catalog `astorb.dat` of the Lowell observatory.⁴

Our algorithm succeeded nearly always. When using the standard `DOUBLE` floating-point arithmetic, the self-test conditions listed above were failed only once per 25000 orbit pairs. In case of such a warning the first attempt was to rerun the same algorithm interchanging the orbits \mathcal{E} and \mathcal{E}' . Since the method treats orbits asymmetrically, this usually helps. Double-warnings occurred in our test once per 2.5×10^6 orbit pairs.

We note that if the algorithm returns a bad self-diagnostic flag, this does not yet mean that it failed to compute the MOID and the result is necessarily wrong or just absent. One of the reasons for a warning is that some root z_k (not even necessarily related to the global minimum) is worse than the required least accuracy δ_{\max} . But worse does not mean necessarily useless. This just means that the result needs an attention and probably needs a more detailed investigation using different other methods to confirm or refine the results. Occurrences when the resulting MOID appears entirely wrong and has unacceptable accuracy, represent only a small fraction of all those cases when the warning was reported.

We also tested the Gronchi FORTRAN code in the same setting. We found only two orbit pairs for which it failed with a error and no-result, and swapping the orbits did not help. A single-fail case, when the first attempt to compute MOID failed, but swapping the orbits did help, occurred once per $\sim 3 \times 10^5$ MOID computations. For the majority of orbit pairs this algorithm gave some numeric MOID value at least, but in itself this does guarantees that all these values are accurate.

We provide a comparison of our new algorithm with the Gronchi code in Fig. 1. We compute the differences of the Gronchi MOID minus the MOID obtained by our new algorithm in two settings. In the first case, we run both algorithms for each orbit pair twice, to compute $\text{MOID}(\mathcal{E}, \mathcal{E}')$ and $\text{MOID}(\mathcal{E}', \mathcal{E})$. With the Gronchi code, we select the minimum MOID between the two, and for our new code we select the best-accuracy MOID. If Gronchi algorithm failed with no-result in one of the two runs, the cor-

⁴See url <ftp://ftp.lowell.edu/pub/elgb/astorb.html>.

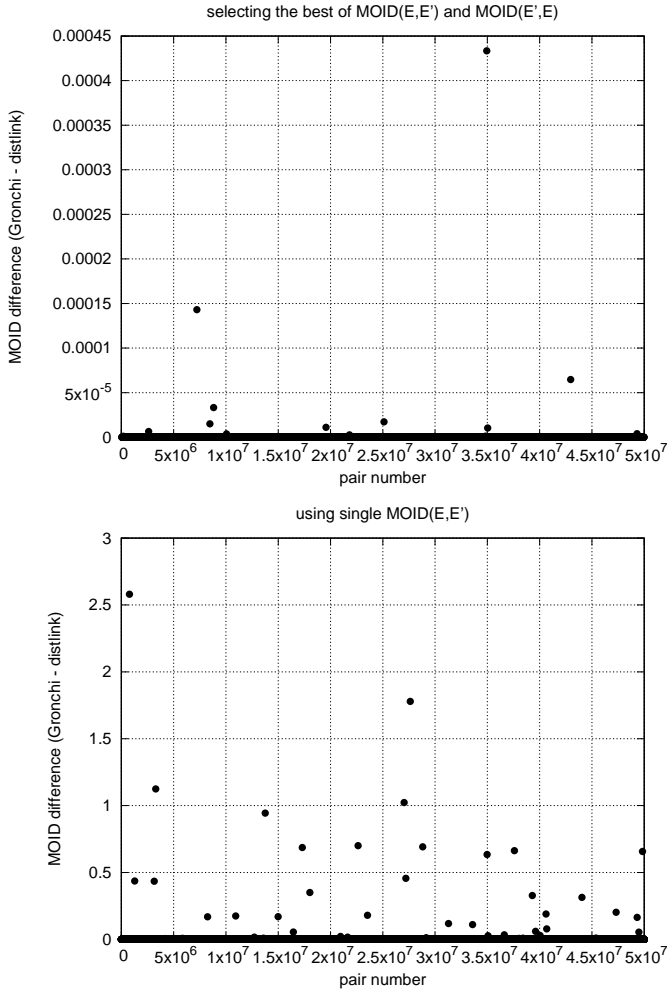


Figure 1: The difference between MOID values computed by the Gronchi’s code and by our new algorithm (labelled as `DISTLINK`). Top: comparing results improved by orbits interchanging and selecting the best MOID of the two. Bottom: using only a single MOID value for comparison. To reduce the figure file size, we removed from the both graphs all differences below 10^{-13} AU in absolute magnitude. In these conditions, no points were revealed below the abscissa, i.e. `DISTLINK` always provided smaller MOID value than the Gronchi’s code. See text for a detailed explanation.

responding MOID value was ignored, and only the other one was used. If both values of the MOID obtained by Gronchi’s algorithm were failed, this orbit pair itself was ignored. Additionally, if our new algorithm reported a warning, we either ignored this MOID in favour of the other value, or invoked the fallback algorithm from Sect. 6, if that second MOID estimate appeared unreliable too. The MOID difference between the Gronchi code and new algorithm was then plotted in the top panel of Fig. 1. In the

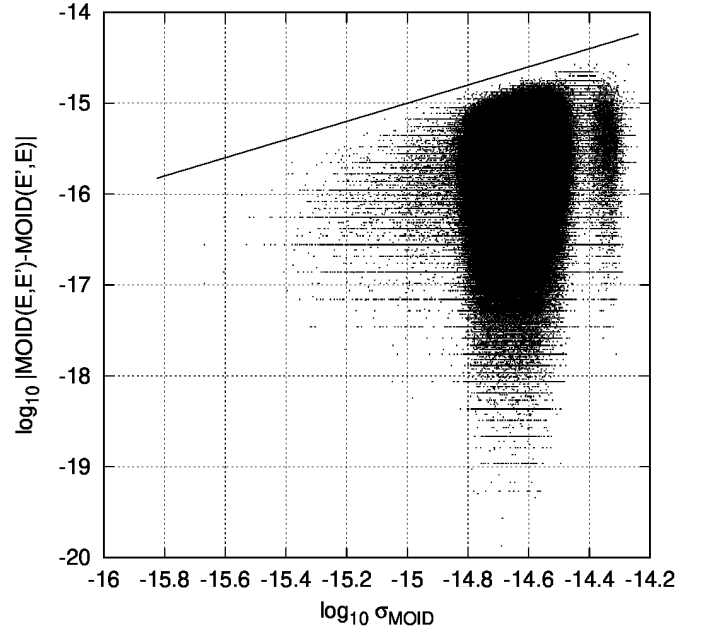


Figure 2: Distribution of the estimated uncertainties σ_{MOID} versus an empiric error measure $|\text{MOID}(\mathcal{E}, \mathcal{E}') - \text{MOID}(\mathcal{E}', \mathcal{E})|$, for the test case of 10^8 orbital pairs (see text). The inclined line labels the main diagonal (abscissa equals ordinate). All simulated dots fell below this line. The computations were done in the `DOUBLE` floating-point arithmetic, AMD FX configuration.

second setting, we plainly performed just a single MOID computation for each orbit pair without orbit interchange, either using the Gronchi code or our new algorithm. Orbit pairs for which Gronchi code failed or our algorithm reported a warning, were ignored and removed. The corresponding MOID difference is plotted in the bottom panel of Fig. 1.

We may see that there are multiple occurrences when Gronchi code obtained clearly overestimated MOID value (i.e., it missed the true global minimum). But all the cases, in which Gronchi algorithm produced smaller MOID than our library, correspond to the MOID difference of $\sim 10^{-13}$ AU at most, with $\sim 10^{-16}$ AU in average. So all these occurrences look like some remaining round-off errors (possibly even in the Gronchi code rather than in `DISTLINK`). Therefore, we did not find an occurrence in which `DISTLINK` would yield clearly wrong MOID value without setting the unreliability flag.

In Fig. 2 we compare the quadrature sum of the reported MOID uncertainties,

$\sigma_{\text{MOID}} = \sqrt{\sigma_{\text{MOID}(\mathcal{E}, \mathcal{E}')}^2 + \sigma_{\text{MOID}(\mathcal{E}', \mathcal{E})}^2}$, with the difference $|\text{MOID}(\mathcal{E}, \mathcal{E}') - \text{MOID}(\mathcal{E}', \mathcal{E})|$ that can be deemed as an empiric estimate of the actual MOID error. We may conclude that our algorithm provides rather safe and realistic assessment of numeric errors, intentionally a bit pessimistic. We did not met a case with the empiric error exceeding the predicted uncertainty.

From Fig. 3 one can see that we spend, in average, about $n = 5 - 6$ Newtonian iterations per each root. One way how we may further increase the speed of computation is to reduce this number. However, this number is already quite small, so there is no much room to significantly reduce it. On the refining stage the algorithm usually performs just one or two 2D Newtonian iterations in the plane (u, u') . The fraction of occurrences when three or more refining iterations are made is very small and further decreases quickly. The maximum number of refining iterations made in this test was 7.

In Table 1, we present our performance benchmarks for this test application. They were done for the following hardware: (i) Intel Core i7-6700K at 4.0 GHz, (ii) Supermicro server with Intel Xeon CPU E5-2630 at 2.4 GHz, and (iii) AMD 990FX chipset with AMD FX-9590 CPU at 4.4 GHz. The second configuration is rather similar to one of those used by Hedo et al. (2018).

We used either 80-bit LONG DOUBLE floating-point arithmetic or the 64-bit DOUBLE one, and requested the desired accuracy of 2ϵ : $\delta_{\min} \sim 2.2 \times 10^{-19}$ or $\delta_{\min} \sim 4.4 \times 10^{-16}$, respectively. We did not use $\delta_{\min} = 0$, because in the DOUBLE case many CPUs hiddenly perform much of the local computation in LONG DOUBLE precision instead of the requested DOUBLE. Newtonian iterations are then continued to this undesiredly increased level of precision, if $\delta_{\min} = 0$, thus introducing an unnecessary minor slowdown. The least required accuracy δ_{\max} was set to $\sqrt{\epsilon}$ in all of the tests.

All the code was compiled with GCC (either g++ or gfortran) and optimized for the local CPU architecture (`-O3 -march=native -mfpmath=sse`). The Gronchi primary computing subroutine `compute_critical_points_shift()` was called from our C++ program natively, i.e.

without any intermediary file IO wrapping that would be necessary if we used the main program `CP_comp.x` from the Gronchi package.

To accurately measure the time spent purely inside just the MOID computation, and not on the file IO or other algorithmic decorations around it, we always performed three independent runs on the test catalog: (i) an ‘empty’ run without any calls to any MOID algorithm, only iteration over the catalog; (ii) computation of all MOIDs using the algorithm of this paper, without writing results to a file; (iii) same for the Gronchi algorithm. The time differences (ii)-(i) or (iii)-(i) gave us the CPU time spent only inside the MOID computation. We never included the CPU time spent in the kernel mode. We assume this system time likely refers to some memory pages manipulation or other similar CPU activity that appears when the program iteratively accesses data from a big catalog. In any case, this system time would be just a minor addition to the result ($\sim 1 - 2$ per cent at most).

The reader may notice that the hardware can generate huge performance differences, not necessarily owing to just the CPU frequency. Moreover, even the performance on the same AMD machine differs drastically between the DOUBLE and LONG DOUBLE tests. This puzzling difference appears mainly due to slow 80-bit floating-point arithmetic on AMD, not because of e.g. different number of Newtonian iterations per root (which appeared almost the same in all our tests, 5–6 iterations per root).

We conclude that our algorithm looks quite competitive and probably even outperforming the benchmarks obtained by Hedo et al. (2018) for their set of tested algorithms (60–80 μs per orbit pair on a Supermicro/Xeon hardware). They used DOUBLE precision rather than LONG DOUBLE one.

Therefore, our algorithm possibly pretends to be the fastest one available to date, or at least it belongs to the family of the fastest ones. In the majority of cases it yields considerably more accurate and reliable results, usually close to the machine precision, and its accuracy may seriously degrade only in extraordinary rare nearly degenerate cases, which are objectively hard to process.

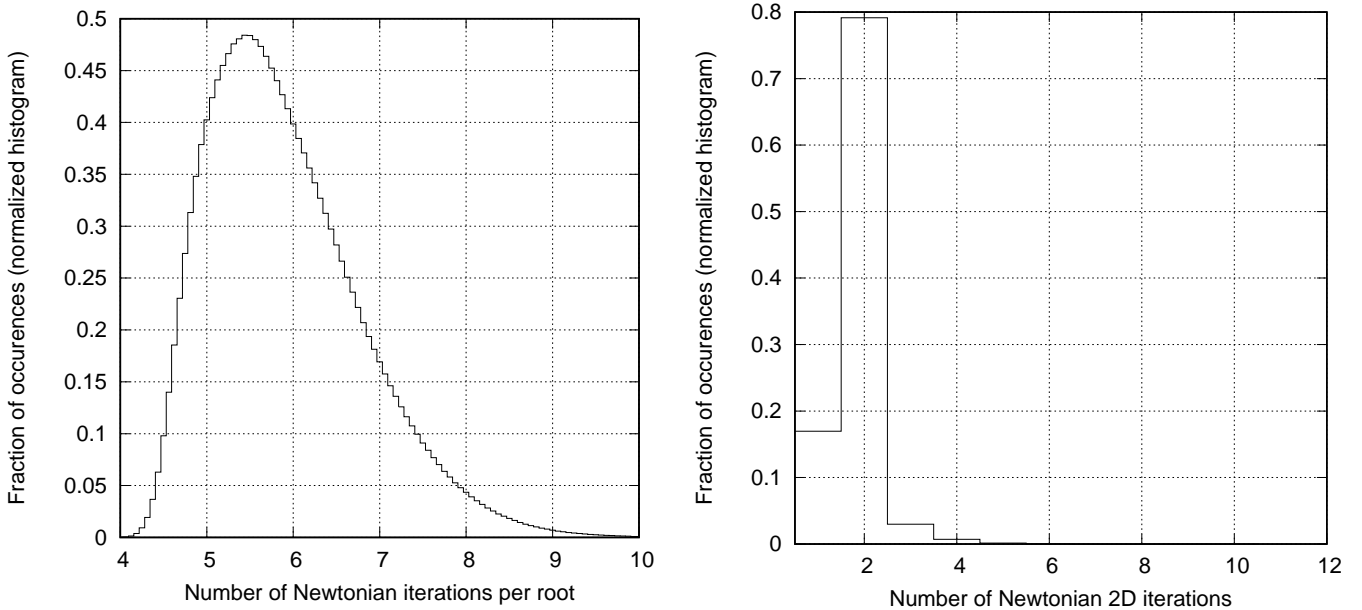


Figure 3: Histogram for the number of Newtonian iterations spent per root (left) and of 2D Newtonian iterations made on the final refine stage (right). The histograms were normalized by the bin width, so they actually render the probability density function for the quantity labelled in the abscissa. The computations were done in the `DOUBLE` floating-point arithmetic, AMD FX configuration.

Table 1: Performance tests on the first 10000 asteroids from the Main Belt: average CPU time per MOID.

Hardware	DOUBLE arithmetic		LONG DOUBLE arithmetic	
	DISTLINK (fast alg.)	Gronchi code	DISTLINK (fast alg.)	Gronchi code
Intel Core i7	24 μ s	36 μ s	77 μ s	NA
Supermicro & Xeon	31 μ s	61 μ s	100 μ s	NA
AMD FX	44 μ s	70 μ s	357 μ s	NA

6. Additional tools

Our main algorithm based on determining the roots of $g(u)$ is fast but might become vulnerable in the rare cases of lost roots. Whenever it signals a warning, alternative algorithms should be used, trading computing speed for better numeric resistance with respect to degeneracies.

In addition to the basic 0D method based on $g(u)$ root-finding, our library implements a “fallback” algorithm of the 1D type, based on the brute force-like minimization of $\tilde{\rho}(u)$. This method is numerically reliable thanks to its simplicity, and its slow speed is not a big disadvantage, because it needs to be run only if the basic fast method failed. In our bench-

marking test it appeared ~ 6 times or ~ 4 times slower than our fast algorithm or the Gronchi code, respectively. But this is likely sensitive to its input parameters.

First of all, the algorithm scans only a restricted range in the u variable, discarding the values where the MOID cannot be attained. The required u range is determined as follows. Using e.g. formulae from (Kholshchevnikov and Vassiliev, 1999a), compute the minimum internodal distance d_Ω . Since MOID is usually attained near the orbital nodes, this quantity and its corresponding orbital positions already provide rather good approximation to the MOID. Then consider two planes parallel to the orbit \mathcal{E}' , and sep-

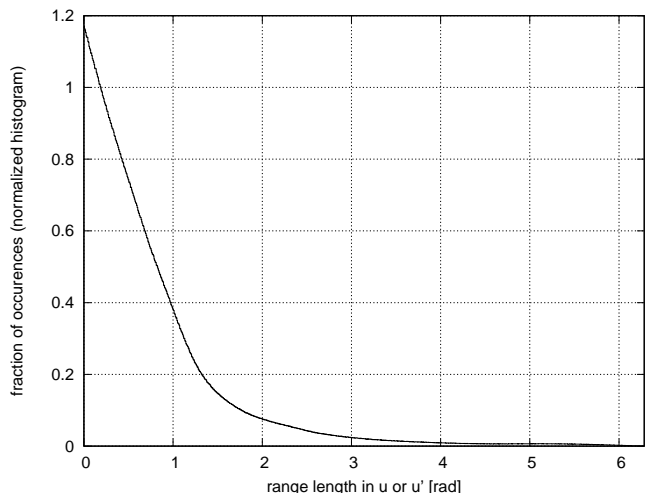


Figure 4: The distribution density of the reduced angular range in u , as obtained for $\sim 10^8$ asteroid pairs.

arated from it by $\pm d_\Omega$. We need to scan only those pieces of orbit \mathcal{E} that lie between these planes, i.e. lie within $\pm d_\Omega$ band from the \mathcal{E}' plane. The points on \mathcal{E} outside of this set are necessarily more distant from \mathcal{E} than d_Ω , so the MOID cannot be attained there. This trick often reduces the u range dramatically. This optimization was inspired by the discussion given in (Hedo et al., 2018). The detailed formulae for the reduced range of u are given in Appendix A.

Moreover, this algorithm automatically selects the optimal orbits order $(\mathcal{E}, \mathcal{E}')$ or $(\mathcal{E}', \mathcal{E})$ to have a smaller angular range to scan. In the case if the cumulative ranges appear equal (e.g. if we occasionally have the full-circle $[0, 2\pi]$ in both cases) then the user-supplied order is preserved.

The efficiency of this approach is demonstrated in Fig. 4, where we plot the distribution density for the total range length obtained, as computed for our test case of $10^4 \times 10^4$ asteroid pairs. The fraction of the cases in which this range could not be reduced at all (remained at $[0, 2\pi]$) is only $\sim 2\%$, and in the majority of occurrences it could be reduced to something well below 1 rad. The efficiency of the reduction increases if MOID is small. Then the total scan range may be reduced to just a few degrees.

The minimization of $\tilde{\rho}(u)$ is based on subsequent sectioning of the initial angular range for u . The user can set an arbitrary sequence of integer numbers $n_1, n_2, n_3, \dots, n_p$ that define how many segments are considered at different stages. The initial angular

range is partitioned into n_1 equal segments separated by the equidistant nodes u_k , and the node with a minimum $\tilde{\rho}(u_k)$ is determined. We note that the input parameter n_1 is always interpreted as if it corresponded to the entire $[0, 2\pi]$ range, even if the actual scan range is reduced as described above. The segment length on the first step is normally set to $h_1 = 2\pi/n_1$ regardless of the scan range, unless this scan range is itself smaller than h_1 . On the second stage, the segment $[u_{k-1}, u_{k+1}]$ surrounding the minimum u_k is considered. It is sectioned into n_2 equal segments, and the node corresponding to the minimum $\tilde{\rho}(u_k)$ is determined again. On the third stage, the segment $[u_{k-1}, u_{k+1}]$ is sectioned into n_3 smaller segments, and so on. On the k th stage, the length of the segment between subsequent nodes is reduced by the factor $2/n_k$, so only $n_k \geq 3$ are meaningful. Starting from the stage number p , the segments are always partitioned into n_p subsegments, until the global minimum of $\tilde{\rho}(u)$ is located with a desired accuracy in u and ρ . It is recommended to set n_1 large enough, e.g. ~ 1000 , in order to sample the objective function with its potentially intricate variations densely enough, whereas the last n_p can be set to 4, meaning the bisection.

We notice that this method was not designed for a standalone use. It was not even supposed to be either more reliable or more accurate in general than our primary fast method. It was supposed to provide just yet another alternative in rare special cases when the primary method did not appear convincingly reliable. Its practical reliability depends on the input parameters very much: too small n_1 may lead to frequent loosing of local minima in $\tilde{\rho}(u)$, if they are narrow. Hence we may miss the correct global minimum sometimes. But this effect can be always suppressed by selecting a larger n_1 . In our tests, with $n_1 = 1000$ this algorithm generated one wrong MOID per ~ 3000 trials, so it is not recommended for a general sole use. This could be improved by implementing an adaptive sampling in the u variable, e.g. depending on the derivative $|\tilde{\rho}'|$, but we did not plan to go that far with this method. We note that narrow local minima of ρ are, informally speaking, in some sense antagonistic to almost-multiple critical points, so this fallback algorithm is vulnerable to rather different conditions than our primary fast

method. Therefore it can serve as a good complement to the latter.

Also, we include in the library several fast tools that may appear useful whenever we need to actually compute the MOID only for those object that are close to an orbital intersection. These tools may help to eliminate most of the orbit pairs from the processing. The first one represents an obvious pericenter–apocenter test: $\text{MOID} \geq a(1 - e) - a'(1 + e')$, and $\text{MOID} \geq a'(1 - e') - a(1 + e)$. If any of these quantities appeared positive and above some upper threshold MOID_{\max} then surely $\text{MOID} > \text{MOID}_{\max}$, and one may immediately discard such orbital pair from the detailed analysis.

Our library also includes functions for computing the so-called linking coefficients introduced by Kholshchevnikov and Vassiliev (1999a). The linking coefficients are functions of two orbits that have the dimension of squared distance, like $|\mathbf{r} - \mathbf{r}'|^2 = 2aa'\rho$, and they are invariable with respect to rotations in \mathbb{R}^3 . Kholshchevnikov and Vassiliev (1999a) introduced three linking coefficients that should be selected depending on whether the orbits are (nearly) coplanar or not. See all the necessary formulae and discussion in that work.

For our goals it might be important that at least one of these linking coefficients, $l_1 = d_1d_2$, can be used as an upper limit on the MOID. It represents a signed product of two internodal distances from (A.6), so the squared MOID can never be larger than $|l_1|$. This allows us to limit the MOID from another side, contrary to the pericenter–apocenter test. Moreover, based on l_1 we introduce yet another linking coefficient defined as

$$l'_1 = \min(|d_1|, |d_2|)^2 \text{sign } l_1. \quad (45)$$

This modified l_1 provides even tighter upper limit on the squared MOID, but still preserves the sign that indicates the orbital linkage in the same way as l_1 did.

It is important for us that all linking coefficients are computed very quickly in comparison to any MOID algorithm, because they are expressed by simple elementary formulae.

The linking coefficients were named so because their original purpose was to indicate whether two orbits are topologically linked like two rings in a chain,

or not. The intermediate case between these two is an intersection, when the linking coefficient vanishes together with the MOID. Therefore, these indicators can be potentially used as computationally cheap surrogates of the MOID. But in addition to measuring the closeness of two orbits to an intersection, linking coefficients carry information about their topological configuration. Also, these quantities can be used to track the time evolution of the mutual topology of perturbed non-Keplerian orbits, for example to locate the moment of their intersection without computing the MOID.

7. Further development and plans

Yet another possible way to extend our library is to implement the method by Baluyev and Kholshchevnikov (2005) for computing the MOID between general confocal unperturbed orbits, including hyperbolic and parabolic ones. This task can be also reduced to finding real roots of a polynomial similar to $\mathcal{P}(z)$.

In a future work we plan to provide statistical results of applying this algorithm to the Main Belt asteroids, also including the comparison of the MOID with linking coefficients and other indicators of orbital closeness.

Acknowledgements

This work was supported by the Russian Science Foundation grant no. 18-12-00050. We express gratitude to the anonymous reviewers for the fruitful comments and useful suggestions on the manuscript.

Appendix A. Reducing the scan range for the eccentric anomaly

Let us introduce $\mathbf{R}' = \mathbf{P}' \times \mathbf{Q}'$, which is a unit vector orthogonal to the orbital plane of \mathcal{E}' . The vectors \mathbf{P}' , \mathbf{Q}' , \mathbf{R}' form an orthonormal basis in \mathbb{R}^3 . Then from (22) let us compute the dot-product

$$(\mathbf{r} - \mathbf{r}')\mathbf{R}' = aPR'(\cos u - e) + aSR' \sin u, \quad (\text{A.1})$$

which represents a projection of the distance vector $\mathbf{r} - \mathbf{r}'$ on the basis vector \mathbf{R}' . Note that the dot-product

$\mathbf{r}'\mathbf{R}'$ is always zero. Now, we need this distance projection to be within $\pm d_\Omega$ from zero, because otherwise the absolute distance can be only larger than d_Ω . This yields two inequality constraints

$$ePR' - \frac{d_\Omega}{a} \leq PR' \cos u + SR' \sin u \leq ePR' + \frac{d_\Omega}{a}, \quad (\text{A.2})$$

implying an elementary trigonometric equation that can be solved via arcsines.

The final set of computing formulae can be expressed as follows. Let us introduce the vector

$$\mathbf{W} = \mathbf{R} \times \mathbf{R}', \quad W = |\mathbf{W}| = \sin I, \quad (\text{A.3})$$

which is directed to the ascending node of \mathcal{E}' assuming reference \mathcal{E} . The angle I is the mutual inclination between the orbits. Then determine the angle θ from

$$\cos \theta = (PW)/W, \quad \sin \theta = (QW)/W. \quad (\text{A.4})$$

It represents the true anomaly on \mathcal{E} , where that ascending node is located. Basically, θ is the angle between \mathbf{P} and \mathbf{W} , counted positive in the direction of \mathbf{Q} . The location on the other orbit θ' can be determined in a similar way. Explicit formula for the scalar product PW is given in (Kholshchikov and Vassiliev, 1999a) via orbital elements, though we prefer to multiply the vectors directly, using the following expression for \mathbf{W} :

$$\begin{aligned} \mathbf{W} = \{ & \cos i \sin i' \cos \Omega' - \sin i \cos i' \cos \Omega, \\ & \cos i \sin i' \sin \Omega' - \sin i \cos i' \sin \Omega, \\ & \sin i \sin i' \sin(\Omega' - \Omega) \}. \end{aligned} \quad (\text{A.5})$$

After that let us compute

$$\begin{aligned} d_1 &= \frac{p}{1 + e \cos \theta} - \frac{p'}{1 + e' \cos \theta'}, \\ d_2 &= \frac{p}{1 - e \cos \theta} - \frac{p'}{1 - e' \cos \theta'}, \\ d_\Omega &= \min(|d_1|, |d_2|), \end{aligned} \quad (\text{A.6})$$

where p and p' are orbital parameters, $p = a(1 - e^2)$.

Now, the inequalities (A.2) may be simplified if we decompose the vectors \mathbf{W} and \mathbf{R}' in the basis $\{\mathbf{P}, \mathbf{Q}, \mathbf{R}\}$:

$$\begin{aligned} \mathbf{W} &= \{PW, QW, RW = 0\}, \\ \mathbf{R}' &= \{PR', QR', RR' = \cos I\}. \end{aligned} \quad (\text{A.7})$$

Writing down the orthogonality condition between \mathbf{W} and \mathbf{R}' and the norm of \mathbf{R}' in these coordinates, we have

$$\begin{aligned} WR' &= PW PR' + QW QR' = 0, \\ R'^2 &= 1 \implies PR'^2 + QR'^2 = W^2. \end{aligned} \quad (\text{A.8})$$

Therefore, we may set $PR' = \mp W \sin \theta$ and $QR' = \pm W \cos \theta$ in (A.2), and the sign choice is not important here.

Finally, let us define the quantity $k \geq 0$ and the angle φ from

$$\begin{aligned} A^2 &= 1 - e^2 \cos^2 \theta, \quad k = \frac{d_\Omega}{aWA}, \\ \sin \varphi &= \frac{\sin \theta}{A}, \quad \cos \varphi = \sqrt{1 - e^2} \frac{\cos \theta}{A}, \end{aligned} \quad (\text{A.9})$$

and (A.2) becomes

$$e \sin \varphi - k \leq \sin(\varphi - u) \leq e \sin \varphi + k. \quad (\text{A.10})$$

In general, we have three types of solution for u .

1. If $|e \sin \varphi| < |1 - k|$ and $k < 1$ then we have two small segments for u near the nodes, defined as $[\varphi - \arcsin(e \sin \varphi + k), \varphi - \arcsin(e \sin \varphi - k)]$ and $[\varphi + \pi + \arcsin(e \sin \varphi - k), \varphi + \pi + \arcsin(e \sin \varphi + k)]$;
2. If $|e \sin \varphi| < |1 - k|$ and $k \geq 1$ then we have the entire circular range $[0, 2\pi]$ for u .
3. If $|e \sin \varphi| \geq |1 - k|$ then there is just one big segment for u that covers angles roughly from one node to another, defined as either $[\varphi + \arcsin(e \sin \varphi - k), \varphi + \pi - \arcsin(e \sin \varphi - k)]$, if $\sin \varphi > 0$, or $[\varphi - \arcsin(e \sin \varphi + k), \varphi + \pi + \arcsin(e \sin \varphi + k)]$, if $\sin \varphi < 0$;

In practice, the first type of occurrence is the most frequent one, so the speed improvement is dramatic. Notice that for $W \rightarrow 0$ (coplanar orbits) the angle θ formally becomes undefined, but this is not important because then $k \rightarrow \infty$ and we just obtain the full-circle range $[0, 2\pi]$ for u . So the degenerate case $W \approx 0$ is not a big numeric issue in practice.

References

- Armellin, R., di Lizia, P., Berz, M., Makino, K., 2010. Computing the critical points of the distance function between two Keplerian orbits via rigorous global optimization. *Celest. Mech. Dyn. Astron.* 107, 377–395.

- Baluyev, R.V., Kholshchevnikov, K.V., 2005. Distance between two arbitrary unperturbed orbits. *Celest. Mech. Dyn. Astron.* 91, 287–300.
- Dybczyński, P.A., Jopek, T.J., Serafin, R.A., 1986. On the minimum distance between two Keplerian orbits with a common focus. *Celest. Mech.* 38, 345–356.
- Gronchi, G.F., 2002. On the stationary points of the squared distance between two ellipses with a common focus. *SIAM J. Sci. Comput.* 24, 61–80.
- Gronchi, G.F., 2005. An algebraic method to compute the critical points of the distance function between two Keplerian orbits. *Celest. Mech. Dyn. Astron.* 93, 295–329.
- Hedo, J.M., Ruíz, M., Peláez, J., 2018. On the minimum orbital intersection distance computation: a new effective method. *MNRAS* 479, 3288–3299.
- Kholshchevnikov, K., Vassiliev, N., 1999a. On linking coefficient of two Keplerian orbits. *Celest. Mech. Dyn. Astron.* 75, 67–74.
- Kholshchevnikov, K., Vassiliev, N., 1999b. On the distance function between two Keplerian elliptic orbits. *Celest. Mech. Dyn. Astron.* 75, 75–83.
- Sitarski, G., 1968. Approaches of the parabolic comets to the outer planets. *Acta Astronomica* 18, 171–195.